Chapter 5
Mathematical model validation for gas solid flow in vertical pipe.

Validation of the mathematical model will be treated in this chapter. Gas-solid particles flow model in cylindrical coordinate as described in section 3.3 is employed in computation. Computed results are then compared with experimental data to evaluate the validity of the model. Alternative structure of flow model, comprising of different turbulence models and their appropriate terms, are validated and chosen in the sense of its capability in predicting the flow. However, prior to validate the model, CFD software and instruction procedure employed in computation are described as preliminary.

5.1 CFD software and instruction procedure

5.1.1 CFD Software structure

A CFD software PHOENICS 2.1 is employed in this study. This PC based software consists of two essential computer codes and two auxiliaries one.

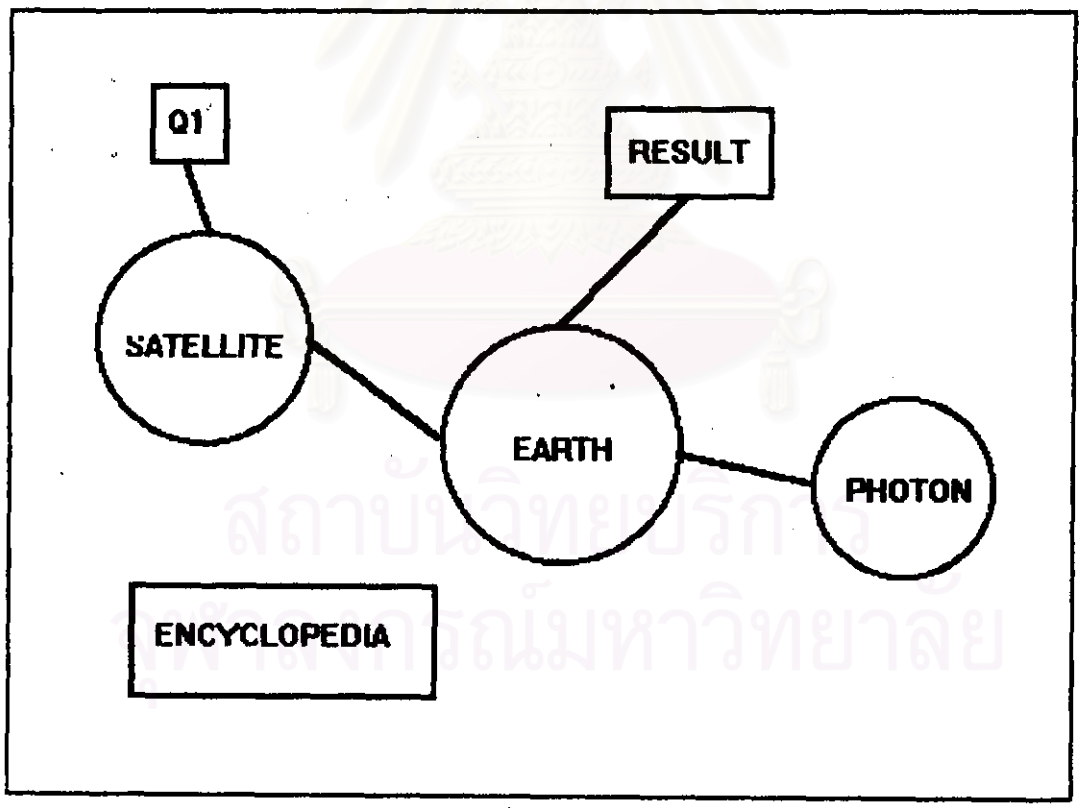

Figure 5.1

PHOENICS COMMANDER structure

The essential one are a PRE-processor called SATELLITE and a Processor called EARTH. The auxiliary are a POST-processor called PHOTON and AUTOPLOT and a separated self reference and instruction program called ENCYCLOPEDIA. Brief description of their functions are as follows;

SATELLITE is an interpreter, it turn instruction from Q1 files or SATLIT menu provided by user into data file containing instruction which EARTH can understand and obey.

SATTELITE may receives its instruction from user in several ways including;
- reading instruction file from SATLIT MENU provided by user.
- reading instruction from Q1 file provide by user.
-receiving keyboard input during an interactive session with user.
-some combination of above.

EARTH contain the main flow-simulating software: it thus incorporates coding sequences which represent the relevant laws of physics applied to elements of material distributed in space and time.

EARTH reads the data file provided by SATELLITE and executes the corresponding computations; it then produces an output file called RESULT, which the user can read, and also (when so instructed) a file of result called PHIDA, which can be read by PHOTON, or by EARTH itself when a new run is started.

The PHOTON code is an interactive program which picks up the PHIDA file written by EARTH and then, in response to instructions entered by user , represents the computed grid and flow pattern graphically on the screen.

5.1.2 Computational instruction procedure

User can instruct PHOENICS to perform flow simulation by;
1. Writing instruction using PIL (PHOENICS Input Language) command directly in Q1 file
2. Setting instruction via SATELLITE MENU.

The instruction data contain 24 groups of data. In this study all instructions are specified via Q1 file. The instruction procedure is as follows;

The flow title and preliminary note can be specified in GROUP 1 Run title and other preliminaries . In this study some variables are declared in this group for ease of changing .

Grid and coordinate structure in computational flow domain can be specified through GROUP 2 Transient :time step specification and GROUP 3, 4 AND 5 : x-, y-, and z- direction grid specification.

In this study a circular pipe flow domain is discretized into two dimensional-cylindrical coordinate grid system. GROUP 2 is not activated in this study since the flow considered is steady. The cylindrical coordinate is activated by setting logic

command "CARTESIAN=F", F denotes false, logically. Now x-direction grid become angular direction, y-direction become radial direction, z-direction become axial direction. For flow domain studied which is two dimensional domain in radial and axial direction, amount of angular grid is set to unity while amount of radial and axial direction grids are specified as appropriate. In each set of grid specification, two sets of information are required, grid amount and total distance. It should be noted that flow direction in this study is vertical so the flow is axisymetric, only one radial half of pipe contain adequate flow field information. The grid and dimension specification of the simulation will be shown case by case under heading "Computational domain".

Variable setting and solution procedure are specified via GROUP 7. Variable solved, stored and named and GROUP 8. Differential equation term and device.

For two phase flow, IPSA is activated by setting the logic command "ONEPHASE=F" in GROUP 7. Once IPSA is activated, pairing of variables between the phases are also arranged by SATELLITE module in the notation 1 and 2 such as W1 and W2 or R1 and R2. Turbulence model is specified in GROUP 7. In this study, k- ε model is activated by command TURMOD(KEMODL). Elliptic or parabolic computation option is selected in GROUP 7 via PARAB=T for parabolic option or elliptic option by default.

Unless otherwise specified in GROUP 8, finite volume equation system, interpolation rules and solution procedure of IPSA as described in Chapter 4 are called for as default. In this study, conventional IPSA available in PHOENICS2.1 is employed in computation.

Fluid and hydrodynamic property of both phases are specified in GROUP 9 Properties of medium

For carrier phase (or gas phase), its density, laminar viscosity are specified. Turbulence diffusivity and other correlation value in turbulence model are already specified once the model is chosen.

For dispersed phase (or solid phase), turbulence momentum diffusivity Schmidt number (δ_p in equation (3.33)), turbulence phase mass diffusivity Schmidt number (Sc_t in equation 3.33) are specified in this group.

Interphase transfer coefficient is formulated in GROUP 10: Interphase-transfer processes and property.

For the flow considered, interphase momentum transfer coefficient of the expression given in equation (3.34) through (3.36) are available in PHOENICS' subroutine and can be activated in this group. Interphase momentum transfer closure is completed once particle diameter and limit of slip velocity are specified.

Initial condition can be specified via GROUP 10 Initializing of variable or porosity field.

In this study, initial field of axial velocities and volume fractions of both phases are specified to uniform field of the value equal to its inlet boundary value.

Boundary condition and source term is specified in GROUP 13 Boundary condition and source term

For inlet boundary, the known boundary variables are mean air velocity and solid loading ratio. Solid volume fraction can then be calculated from equation (3.48). Particle inlet velocity is calculated or specified depending on type of problem. In the validation case which fully developed flow are of interest, particle inlet velocity can be set equal to air velocity since the flow field in acceleration zone is ignored. For pressure profile validation or in airlift application case which flow field in acceleration region is coming in question, particle velocity at inlet boundary must be determined accurately. Calculation procedure of particle velocity at inlet boundary are described in Section 3.3.2c.

For wall boundary of gas phase, the wall function method described in Section 3.3.1d is available in PHOENICS 2.1 and can be activated by PIL command. The effect of particle-wall boundary will be investigated, however, its effect to airlift flow is expected to be negligible as discussed in first paragraph under Section 3.3.2c. The outlet boundary of both phases are specified in order to balance the net mass source in the computational cells adjacent to outlet boundary. For elliptic computation, The outlet boundary pressure has to be specified. Gas phase pressure can be specified in straight-forward manner. Since both phases theoretically share the same pressure, pressure variable P2 in PHOENICS is therefore treated as particle mass source.

The other source terms which are specified in GROUP 13 are gravity field and turbulence extra dissipation terms (P_k, P_ε in equation(3.22) and (3.23)) of Chen-Wood [1986]'s and Mostafa-Mongia[1988]'s model.

Solution control and relaxation devices are specified in GROUP 15 to GROUP 18 as follows;

If elliptic option is activated, a number of sweeps need to be specified in GROUP 15 termination of sweep. If parabolic option is activated, the number of sweep is set to unity and number of hydrodynamic iterations are specified in GROUP 16 termination of iteration . Appropriate number of sweeps and iterations depend on the nature of each numerical problem and some trial and error process have to be performed in order to find out appropriate number of sweeps of which convergence criteria is satisfied.

The under-relaxation is very important for preventing the overshoot value of variable during computation procedure as discussed in Section 4.6.6. In this study, the appropriate under relaxation values range between 0.1 and 0.5 for velocity, volume fraction and turbulence kinetic energy of both phases. These values are specified in GROUP 17 Under-relaxation device.

During computation, it is preferable to terminate computation of some variable when its iteration error reaches a tiny value. The limit of variable error specified in GROUP 18 Limits on variable or increment to them , serve this purpose.

GROUP 20 to 24 are monitor and print out control instructions which is immaterial for this section.

Once all of 24 group instructions are written in Q1 file, it is interpreted by SATELLITE and then computed by EARTH. The computed results are obtained as will be discussed later on.

5.2 Model validation

The reliable mathematical model in predicting gas-particle flow in vertical pipe is the most important task prior to perform further computational experiments of airlift flow. In this Section, computed flow field variables will be validated with published experimental data of Tsuji et al.[1984]. The validated model will be employed for computational experiment study in the next chapter.

5.2.1 Experimental data

The detail of experimental apparatus diagram and experimental method of Tsuji et al.[1984] has been discussed in Section 2.2. In this Section, the experimental data used for validation is illustrated and discussed.

5.2.1a. Axial velocity on radial variation.

Figure 5.2 show axial velocity on radial variation of air and 200 μm particles at mean air velocity 15.6 m/s and 15.3 m/s at solid loading ratio (m = solid mass flow rate/gas mass flow rate) 1.0 and 2.1 respectively. From Figure 5.2, air velocities are higher than particle velocities in the region from pipe centerline to approximately 0.86R where velocities of both phases become approximately equal. In the region from 0.86R to pipe wall (R), particle velocities are higher than air velocities. This phenomena can be described in term of slip velocity (defined as difference of velocity between gas phase and solid phase), for brevity, that slip velocity change its sign from plus (+) to minus (-) at 0.86R. This phenomena can be observed on both solid loading ratios and will be investigated during validation.

Figure 5.3 illustrated axial velocity on radial variation of air and 500 μm particle at mean air velocity 7.96m/s and 8.00 m/s at solid loading ratio 1.1 and 2.0 respectively. The change of slip velocity sign can not be seen in experimental data since it occur very close to the pipe wall. The 500 μm particles velocity profiles are flatter than those of 200μm particle. Flatter air velocity profile can be observed at higher solid loading ratio.

5.21b. Turbulence intensity on radial variation

Turbulence intensity experimental data of air at various solid loading ratio in the presence of 200μm particles are plotted in Figure 5.4. Compare with clean air

flow (m=0.0), the presence of particles cause suppression of turbulence intensity through out the pipe cross section.

Figure 5.5 show turbulence intensity experimental data of air at various solid loading ratios in the presence of 500 μm particles. Compare with clean air flow (m=0.0), The presence of particles tend to promote turbulence intensities near pipe center and cause suppression toward the pipe wall.

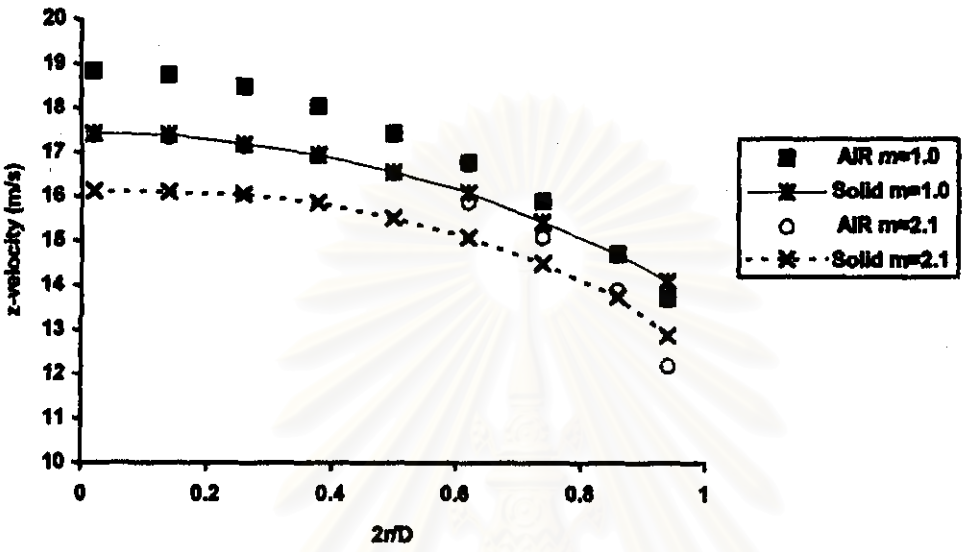

Figure 5.2
Axial velocity profile in radial variation of air and particle in the presence of 200μm particles. Mean air velocity V_z=15.6 m/s for m=1.0,V_z=15.3m/s for m=2.1. Data obtained from Tsuji's et al. [1984].

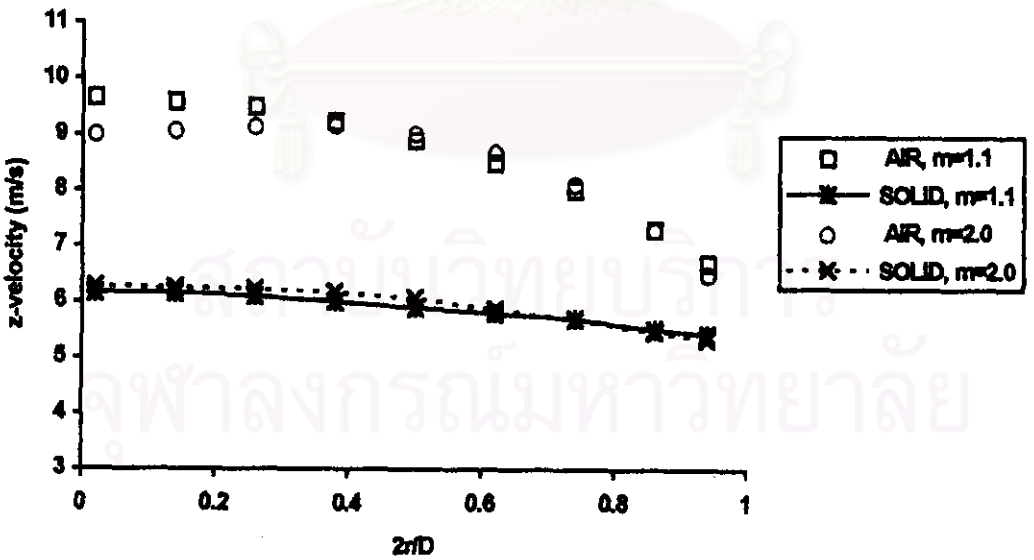

Figure 5.3
Axial velocity profile in radial variation of air and particle in the presence of 500μm particles. Mean air velocity V_z=7.96 m/s for m=1.1,V_z=8.00m/s for m=2.0. Data obtained from Tsuji's et al. [1984].

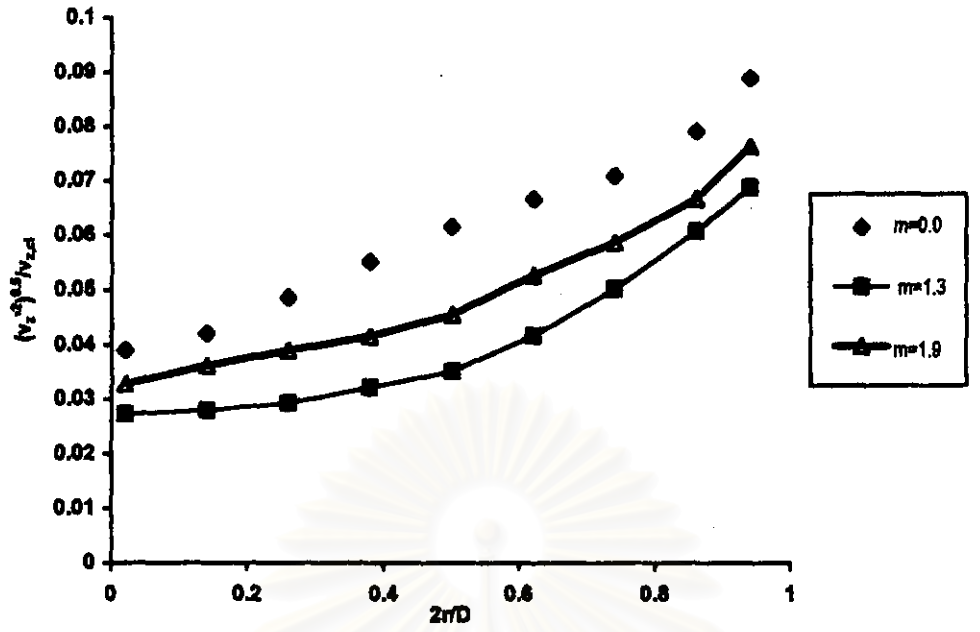

Figure 5.4

Turbulence intensity of air in the presence of 200 μm particles obtained from Tsuji et al.[1984] 's experimental data, pipe flow Reynolds number in all case are approximately comparable, for m=0.0,$v_{z,cl}$=13.4, for m=1.3, $v_{z,cl}$=12.8m/s, for m=1.9, $v_{z,cl}$=11.9 m/s.

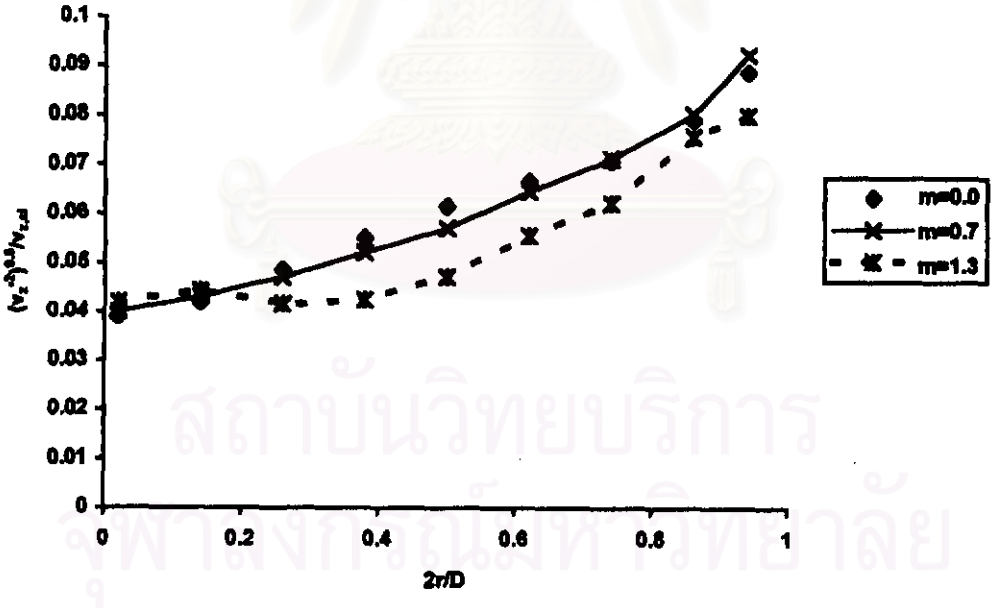

Figure 5.5

Turbulence intensity of air in the presence of 500μm particles obtained from Tsuji et al [1984] 's experimental data, pipe flow Reynolds number in all case are approximately comparable, for m=0.0,$v_{z,cl}$=13.4, for m=0.7, $v_{z,cl}$=12.2, for m=1.3, $v_{z,cl}$=13.3 m/s.

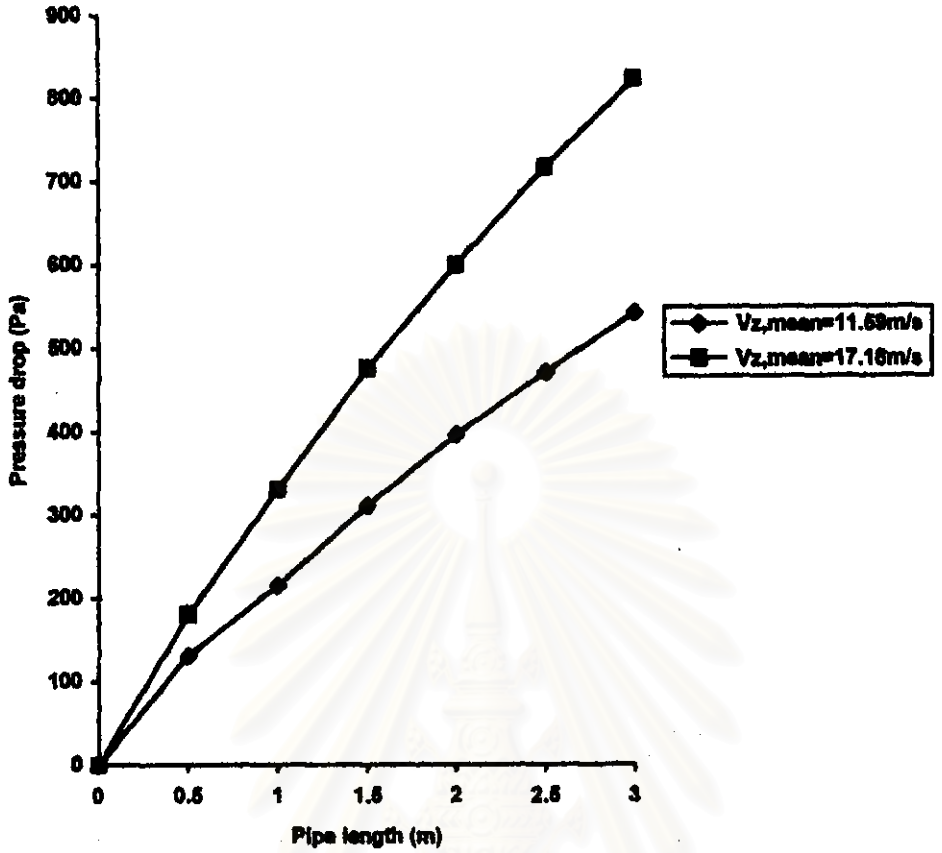

Figure 5.6

Pressure drop distribution along axial direction in the presence of 500μm particles, solid mass flow rate = 3.0×10^{-2} kg/s in both cases, data obtained from Tsuji et al. [1984].

5.2.1c Pressure drop profile

Axial pressure drop profile experimental data can be investigated from Figure 5.6. The profiles illustrate the developing of flow field in acceleration region. The pressure gradient reaches constant when the flow reaches steady state and fully developed. The curvature of pressure drop profile is an important characteristic which need to be investigated.

5.2.2 Model validation : general

The above experimental flow conditions are simulated by CFD technique using PHOENICS2.1. In summary, the flow domain and material properties which are common in all computational cases are as follows;

Computational domain	
Amount of angular grid	1
Angular grid distance	0.1Rad.
Amount of radial grid	25
Radial grid distance	0.5×(30.5mm)
Type of radial grid	Uniform
amount of axial grid	70 and 100
Axial grid distance	70,100×(30.5 mm)
Type of axial grid	Uniform

Table 5.1

Fluid and hydrodynamic property	
Air density	1.178 Kg/m^3
Air laminar viscosity	1.868×10^{-5} kg/m.s
Particle density	1020 kg/m^3
Particle phase mass Schmidt number(Sc_t)	0.7
Particle shear stress Schmidt number(δ_p)	1.697

Table 5.2

Particle size, Air mean velocity at inlet boundary and solid loading ratio are set following experimental flow conditions.

The above flow information is written in Q1 file as outlined in **section5.1.2.** The Q1 file of various computational cases are attached in APPENDIX B1-B3 where instruction notes are also put in for clarification. After Q1 file is written, it was interpreted by SATELLITE and then computed by EARTH.

The computed results of velocity, volume fraction of both phases together with k, ε, and turbulence viscosity of gas phase are printed in RESULT file in conventional SI unit and can then be analyzed directly. In order to validate the model for turbulence intensity (or normalized fluctuation velocity) prediction, the computed results of Turbulence kinetic energy (k) require some mathematical treatment as follows;

Turbulence intensity (I) is defined as ;

$$I = \frac{\left(v'^2\right)^{0.5}}{\overline{V}} \tag{5.1}$$

Subscripts are omitted in (5.1) to denote "any" direction. There is no strict recommendation for $\overline{V}$ as it may be centerline velocity or mean velocity. turbulence intensity can be written in the term of turbulence kinetic energy as follows;

From definition of Turbulence kinetic energy

$$k = 0.5\left(v_x'^2 + v_y'^2 + v_z'^2\right) \tag{5.2}$$

For k-ε model, isotropic property is assumed;

$$v_x'^2 = v_y'^2 = v_z'^2 \tag{5.3}$$

Therefore

$$k = 0.5\left(3v'^2\right) \tag{5.4}$$

Or, in term of fluctuation velocity

$$v' = \sqrt{\frac{k}{1.5}} \tag{5.5}$$

Substitute into equation (5.1)

$$I = \frac{\sqrt{k/1.5}}{\bar{V}} \tag{5.6}$$

Equation(5.6) transform turbulence kinetic energy (k) to turbulence intensity ready to compare with experimental data.

During validation procedure, the computed results are qualitatively and quantitatively compared with experimental data. Qualitative comparison is performed by evaluating the similarity of shape and behavior of profile. Quantitative comparison need some error calculation in order that various set of data can be compared on the same basis. In satisfying this needs, **radial weighted error** is introduced for cylindrical coordinate as follows;

$$E = \frac{\sum_{i=1}^{N}\left(\left|\frac{X_{literature} - X_{computed}}{X_{literature}}\right|_i \times r_i\right)}{\sum_{i=1}^{N} r_i} \tag{5.7}$$

X is any flow field value, r is the normalized radial distance , i is the point where the data is located.

As all of turbulence models employed in this study are standard and modified k-ε models, "Clean air" validation of single phase-standard k-ε model is performed to confirm its prediction capability. Figure 5.7 and 5.8 show axial velocity profile and turbulence intensity profile on radial variation of "clean air" flow data of Tsuji et al. [1984] versus computed results. The computed results yield a good prediction of velocity profile. However, computed turbulence intensities in the near-wall region are quite lower than experimental data. This is not surprising since the computation is done based on "smooth wall" assumption. The deviation of turbulence intensities near pipe wall can also be observed in Louge et al. [1991] and Bilirgen et al.[1998].

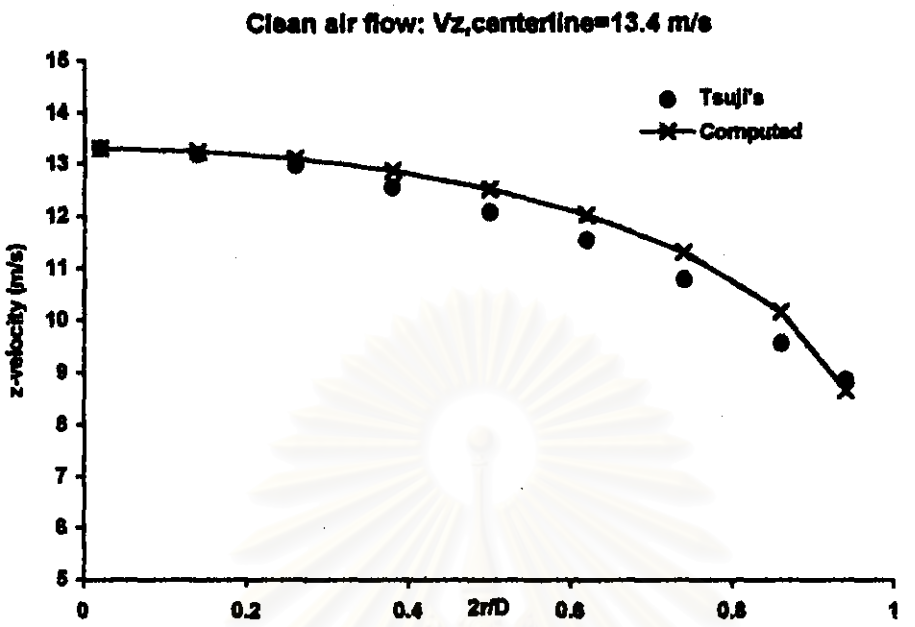

Figure 5.7

Axial velocity on radial variation of Clean air pipe flow , centerline velocity=13.4m/s, Data legend: **Tsuji's** is Tsuji et al. [1984]'s experimental data , **computed** is computed result using standard k-ε model.

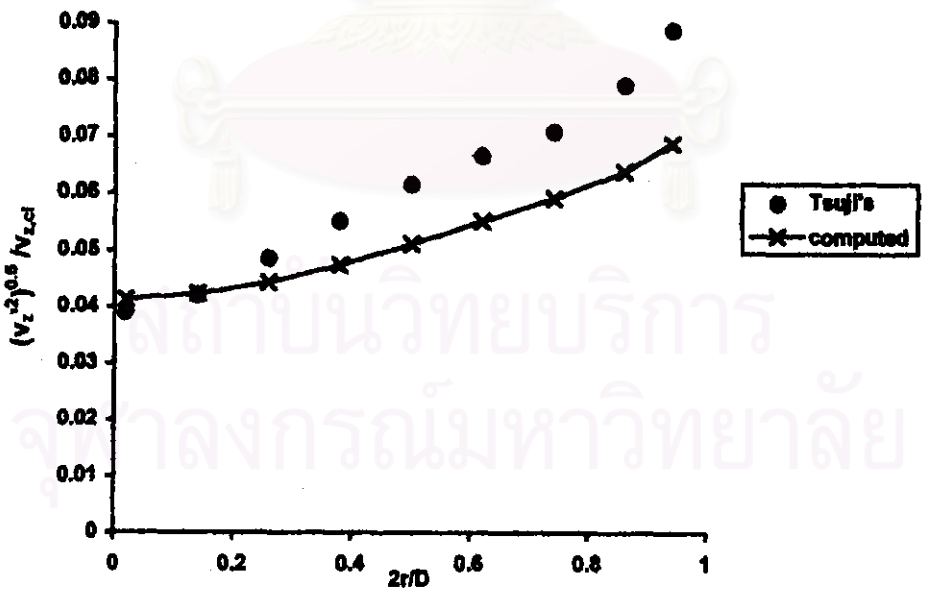

Figure 5.8

Turbulence intensity on radial variation of clean air in pipe flow , centerline velocity=13.4, Data legend: **Tsuji's** is Tsuji et al. [1984]'s experimental data , **computed** is computed result using standard k-ε model.

5.2.3 Model validation: turbulence model validation

In order to validate the mathematical model in predicting fully developed velocity profile of both phases and air turbulence intensity, some simplification of equation set described in Section 3.3 can be reasonably made. Consider turbulence phase mass diffusion term in equation (3.33) and (3.34) can be neglected since volume fraction gradient $\frac{\partial \gamma_s}{\partial r}$ can be assumed zero in fully developed flow region. Moreover, accurate value of particle velocity at inlet boundary is unnecessary as it cause indifferent fully developed flow prediction, even though the inaccurate inlet particle velocity can lead to drastically inaccuracy of flow field values in acceleration region of the pipe. The particle inlet velocity is therefore specified equal to air inlet velocity in validating with fully developed flow field data.

The particle involving in this study is quite massive. The particle-particle interaction is expected dominant. For fully developed flow simulation, including or excluding particle shear stress term of equation (3.34) in computation may yield significantly different results. This effect will be carefully investigated .

There are three turbulence models employed in model validation. All are k-ε based models. Standard k-ε does not account for turbulence promotion/modulation effect due to the presence of particles while Chen-Wood [1986]'s and Mostafa-Mongia [1988]'s do. Equation (3.22) and (3.23) of all three models are employed in this study.

In Figure 5.9, computed air and particle axial velocities of 200μm particles flow in mean air velocity 15.6 m/s at solid loading ratio 1.0 are plotted against the corresponding experimental data which previously shown in Figure 5.2. Each computation is made by excluding particle shear stress term and three turbulence models are employed to investigate its validity.

The advantage of standard k-ε model over the other two in predicting particle velocity profile is noticeable from Figure 5.9. In this flow condition , all computed data seem to be in good agreement with experimental data. The reverse of slip velocity sign near by wall can not be predicted by any of these computations.

In Figure 5.10, computed air and particle axial velocities of 200μm particles flow in mean air velocity 15.3 m/s at solid loading ratio 2.1 are plotted against the corresponding experimental data which previously shown in Figure 5.2. Again, each computation is made by excluding particle shear stress term and three turbulence models are employed to investigate its validity. Compare with Figure 5.9, the more significant difference of computed results among the three turbulence models can be observed in Figure 510. Standard k-ε model employed computation tend to yield better prediction of both air and particle velocity profiles than the other two model. Chen-Wood [1986]'s and Mostafa-Mongia [1988]'s model employed computation seem to yield "steeper" air and particle velocity profiles than Standard k-ε model employed computation in the relative with experimental data.

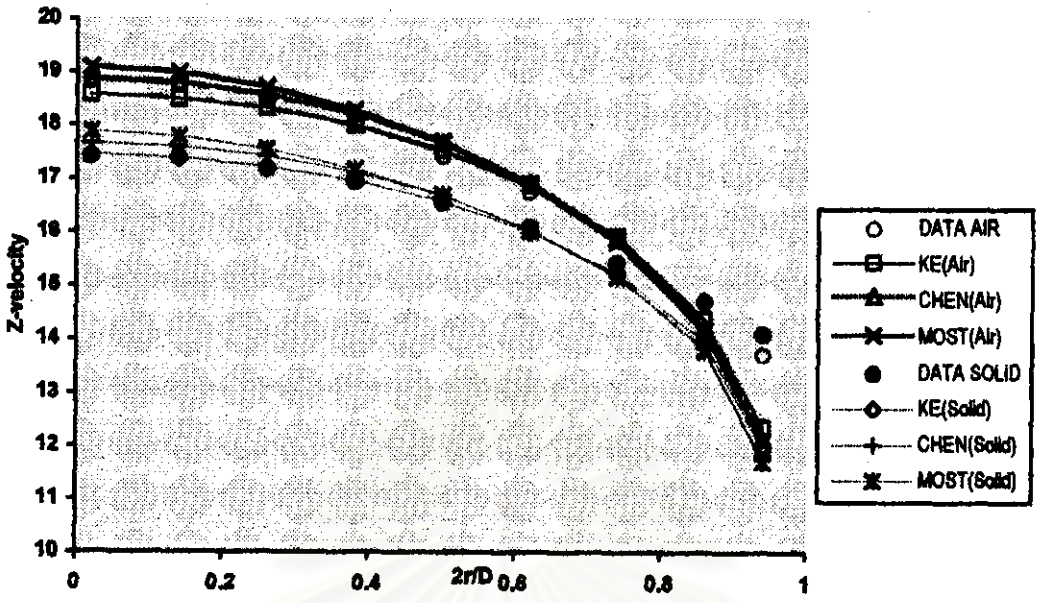

Figure 5.9

Axial velocity profile on radial variation of mean air velocity =15.6 m/s laden with 200μm. particles at solid loading ratio=1.0 , meaning of data legend: Data air and Data solid from Tsuji et.al [1984]'s experimental data, KE(Air) and KE(Solid) are computed value using standard k-ε model,CHEN (Air) and CHEN(Solid) are computed value using Chen-Wood [1986]'s model, MOST(Air) and MOST(Solid) are computed value using Mostafa-Mongia [1988]'s model. Particle shear stress term is excluded from computation.

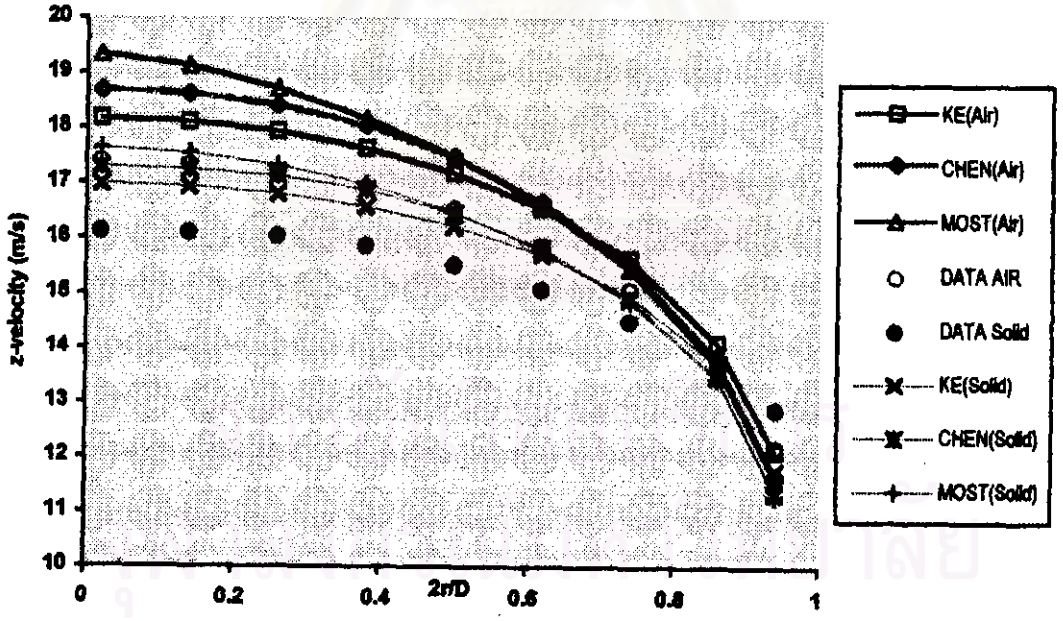

Figure 5.10

Axial velocity profile on radial variation of mean air velocity =15.3 m/s laden with 200μm. particles at solid loading ratio=2.1 , meaning of data legend: Data air and Data solid from Tsuji et.al [1984]'s experimental data, KE(Air) and KE(Solid) are computed value using standard k-ε model, CHEN (Air) and CHEN(Solid) are computed value using Chen-Wood [1986]'s model, MOST(Air) and MOST(Solid) are computed value using Mostafa-Mongia [1988]'s model. Particle shear stress term is excluded from computation.

As observed from Figure 5.10, the reverse sign of slip velocity can not be predicted by computation.

In Figure 5.11, computed air and particle axial velocities of 500μm particles flow in mean air velocity 7.96 m/s at solid loading ratio 1.1 are plotted against the corresponding experimental data which previously shown in Figure 5.3. Each computation is made by excluding particle shear stress term and three turbulence models are employed to investigate its validity.

Standard k-ε model employed computation still yield more favorable result than the other two models in predicting air and particle velocity profiles. However, all three models fail to simulate rather flat profile of experimental particle velocity . All three models perform good prediction for air velocity profiles except, again , at near wall region.

In Figure 5.12, computed air and particle axial velocities of 500μm particles flow in mean air velocity 8.00 m/s at solid loading ratio 2.0 are plotted against the corresponding experimental data which previously shown in Figure 5.3. Each computation is made by excluding particle shear stress term and three turbulence models are employed.

Standard k-ε model employed computation still yield more favorable results than the other two models in predicting air and particle velocity profiles. As was found in Figure 5.11, all three models fail to simulate rather flat profile of experimental particle velocity. For air velocity prediction, standard k-ε model employed computation yield more favorable results significantly than the other two models.

The similar trend can be concluded from the result presented in Figure 5.9 through Figure 5.12. Standard k-ε model employed computation yields more favorable results than the other two models in predicting air and particle velocity profiles in all flow conditions. All mathematical models employed in the above computation can not accurately predict reverse of slip velocity sign and cannot simulate flat profile of 500 μm particle velocity .

In Figure 5.13, computed turbulence intensities (I) of air in the presence of 200 μm particles at solid loading ratio 1.3 are plotted against experimental data. The fluctuation velocities v′ are normalized by centerline axial velocity $V_{z,cl}$. The computation is made by excluding particle shear stress term and three turbulence model are employed .

Experiencing that, from Figure 5.9 and 5.10, standard k-ε employed model computation yield the flattest and approximately nearest centerline velocity to the experimental data, the standard k-ε model employed computation is then performed at mean air velocity 10.84 m/s which give computed air centerline velocity $V_{z,cl}$=13.0 m/s close to 12.8 m/s of experimental data. Keeping mean air velocity in all cases fix, $V_{z,cl}$=13.25 m/s is computed by Chen-Wood employed model and $V_{z,cl}$=13.7 m/s is computed by Mostafa-Mongia [1988] employed model.

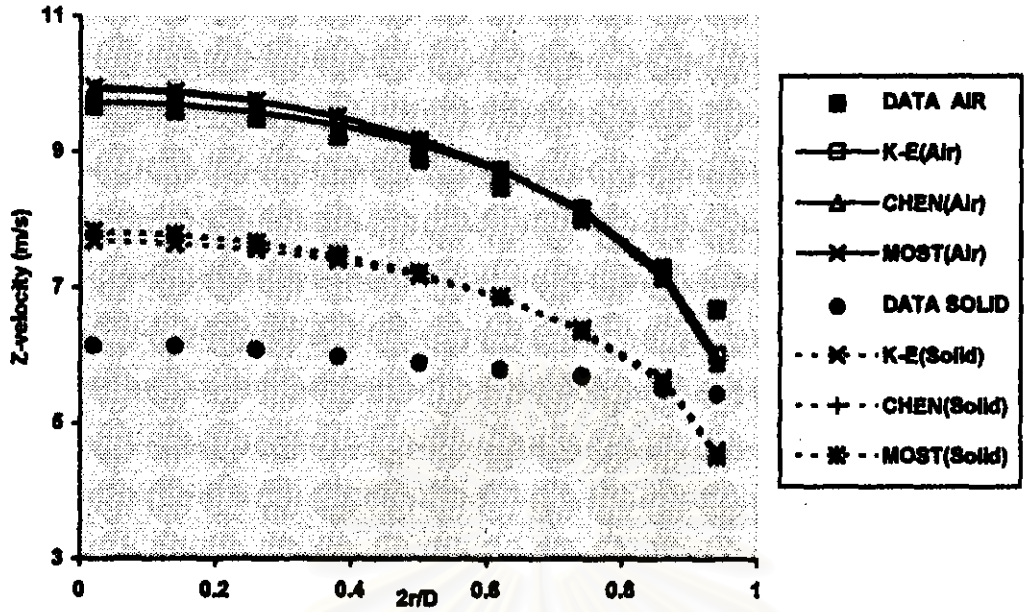

Figure 5.11

Axial velocity profile on radial variation of mean air velocity =7.96 m/s laden with 500μm. particles at solid loading ratio=1.1 , meaning of data legend: Data air and Data solid from Tsuji et.al [1984]'s experimental data, KE(Air) and KE(Solid) are computed value using standard k-ε model, CHEN (Air) and CHEN(Solid) are computed value using Chen-Wood [1986]'s model, MOST(Air) and MOST(Solid) are computed value using Mostafa-Mongia [1988]'s model. Particle shear stress term is excluded from computation.

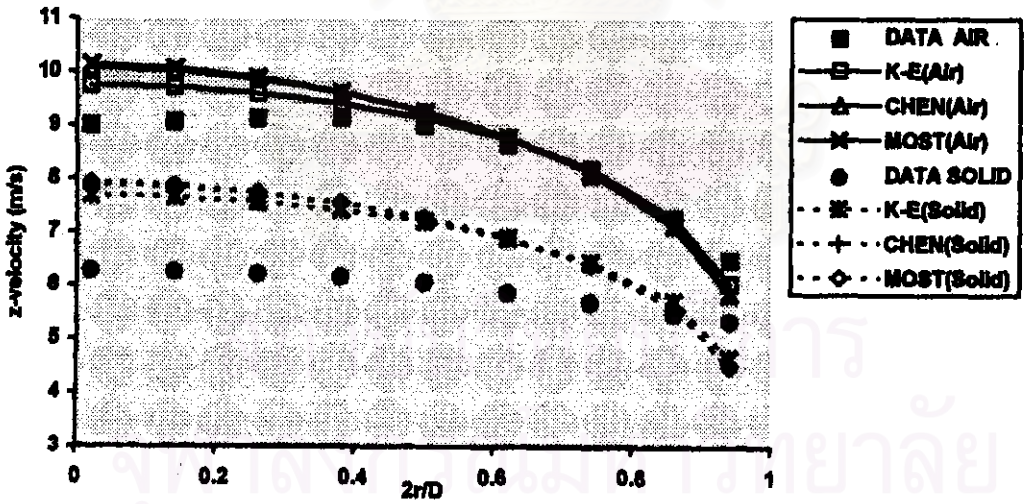

Figure 5.12

Axial velocity profile on radial variation of mean air velocity =8.00 m/s laden with 500μm. particles at solid loading ratio=2.0 , meaning of data legend: Data air and Data solid from Tsuji et.al [1984]'s experimental data, KE(Air) and KE(Solid) are computed value using standard k-ε model,CHEN (Air) and CHEN(Solid) are computed value using Chen-Wood [1986]'s model, MOST(Air) and MOST(Solid) are computed value using Mostafa-Mongia [1988]'s model. Particle shear stress term is excluded from computation.

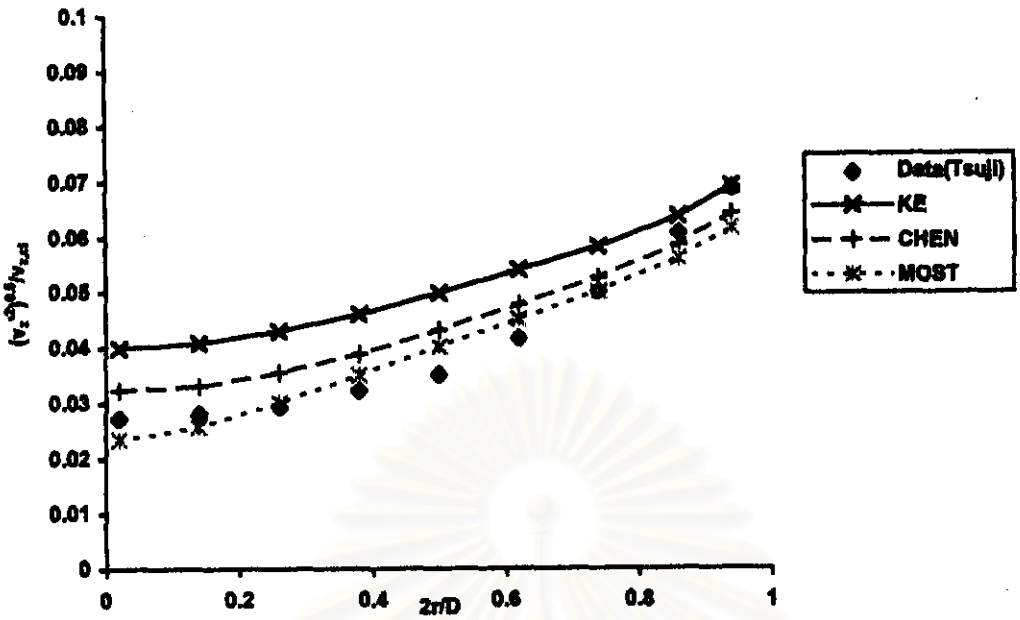

Figure5.13

Turbulent intensity of air in the presence of 200μm particles, m=1.3,data legend: Tsuji; Tsuji et al. [1984]'s experiment data at $v_{z,cl}$=12.8 m/s , KE; Computed result using standard k-ε model at $v_{z,cl}$=13.0 m/s, CHEN; computed result using Chen-Wood [1986]'s model at $v_{z,cl}$=13.25 m/s, MOST; computed result using Mostafa-Mongia [1988]'s model at $v_{z,cl}$=13.7 m/s. Particle shear stress term is excluded in all computations. In all cases, $\bar{V}_z \cong 10.84$ m/s.

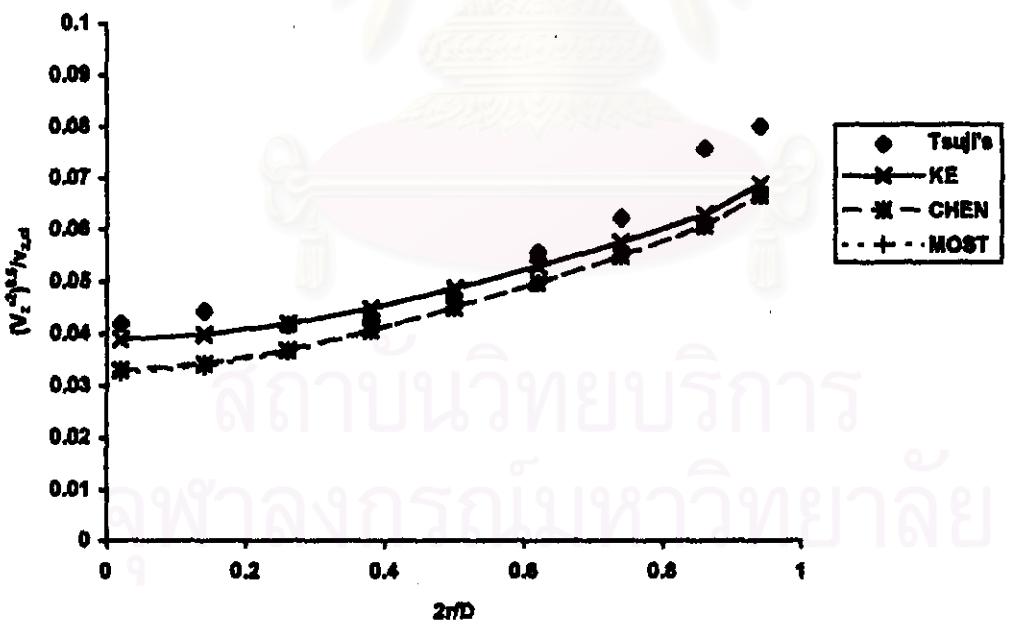

Figure 5.14

Turbulent intensity of air in the presence of 500μm particles, m=1.3,data legend: Tsuji; Tsuji et al. [1984]'s experiment data at $v_{z,cl}$=13.3 m/s , KE; Computed result using standard k-ε model at $v_{z,cl}$=13.33 m/s, CHEN; computed result using Chen-Wood [1986]'s model at $v_{z,cl}$=13.52 m/s, MOST; computed result using Mostafa-Mongia [1988]'s model at $v_{z,cl}$=13.53 m/s. Particle shear stress term is excluded in all computations. In all cases, $\bar{V}_z \cong 11.15$ m/s.

Computed turbulence intensities of standard k-ε employed model in Figure 5.13 are higher than experimental data in the vicinity of pipe center but yield better prediction in the near wall region.Consider the other two models, both show applausable performance in predicting turbulence intensities in the vicinity of pipe center but slightly under predict turbulence intensities in near wall region. Radial weighted error calculated by equation (5.7) for standard k-ε employed model, E=20.6%; for Chen-Wood [1986] employed model, E=11.207%; for Mostafa-Mongia [1988] employed model, E=7.72%. This reveal superior performance of particle source/sink turbulence model in predicting turbulence intensity of air within unrestricted region such as in the vicinity of pipe center of 200μm particle size. However, it should be noted that centerline velocity predicted by both particle source/sink turbulence models are significantly higher than experimental data at the same Reynolds number.

It should be recalled that both particle source/sink turbulence models are correlated from two-phase free jet of 50-200μm particles in high gas Reynolds number at relatively low solid loading ratio (maximum=0.66) experimental data. It is not surprising that both can accurately predict the air turbulence intensities in the region far from wall for 200μm particles.

In Figure 5.14, computed turbulence intensities (I) of air in the presence of 500 μm particle at solid loading ratio 1.3 are plotted against experimental data. The fluctuation velocities v' are normalized by centerline axial velocity $V_{z,cl}$. The computation is made by excluding particle shear stress term and three turbulence model are employed .In all computations, mean air velocity is 11.15 m/s. Computed centerline velocity of standard k-ε employed model is 13.33 m/s close to experimental centerline velocity which is 13.3 m/s. Turbulence intensity profiles computed by standard k-ε model seem to yield better agreement to experimental data than the other two models. Radial weighted error for standard k-ε employed model is E=9.4%, for Chen-Wood's is E=13.3% and for Mostafa-Mongia's is E=13.3%. However the improvement of standard k-ε model prediction performance is only coincident since the computed turbulence intensity profile is equal to single phase computation at the same Reynolds number.

Consider from all validations discussed above, the standard k-ε computation appears more capable for predicting axial velocity profile than the other two models. However validity of standard k-ε model in predicting turbulence kinetic energy can not be confirmed. Comparing among the three models, the standard k-ε model computation is considered more valid in predicting gas-particle pipe flow in the range considered.

5.2.4 Model validation: effect of particle shear stress term

In this section, effect of particle shear stress term is investigated. standard k-ε model employed conservation equation in Section 3.3 including particle shear stress term in equation (3.34) is computed for all cases in this section.

In Figure 5.15 and Figure 5.16, computed axial velocity of both phases of 200 μm particles at solid loading ratio 1.0 and 2.1 are plotted against experimental data in order to investigate effect of particle shear stress. The flow conditions are the same as of Figure 5.9 and Figure 5.10 respectively. Compare computed velocity profiles with Figure 5.9 and Figure 5.10, significant improvement of computed particle velocity profiles in Figure 5.15 and Figure 5.16 can be observed. Radial weighted error decrease from 4.42% of KE(solid) data in Figure 5.9 to 3.62% of KE(solid) data in Figure 5.15 and decrease from 4.34% of KE(solid) data in Figure 5.10 to 2.68% of KE (solid) data in Figure 5.16. Reverse of slip velocity sign occur at r=0.88R on both computed profiles which are in agreement with experimental data. This evidence lead to the conclusion that reverse of slip velocity sign is induced by particle shear stress effect. Particle shear stress is transferred from higher particle velocities in the vicinity of pipe center toward the lower velocities in the vicinity of pipe wall, as a result, particle velocity near wall is elevated.

Figure 5.17 and Figure 5.18 show the effect of particle shear stress term on computed gas and 500μm particles velocity profiles prediction at solid loading ratio 1.1 and 2.0. The flow conditions are the same as of Figure 5.11 and Figure 5.12 respectively. Significant improvement can be observed by comparing Figure 5.17 against Figure 5.11 and Figure 5.18 against Figure 5.12. Radial weighted error decrease from 15.1% of KE(solid) data in Figure 5.11 to 12.74% of KE(solid) data in Figure 5.17 and decrease from 14.16% of KE(solid) data in Figure 5.12 to 12.74% of KE(solid) data in Figure 5.18. These results lead to the conclusion that better particle velocity prediction can be achieved qualitatively and quantitatively by including particle shear stress term into standard k-ε employed conservation equation . Validity of model in particle velocity prediction is essential for solid volume fraction prediction since solid flux is proportional to product of particle velocity and solid volume fraction.

Figure 5.19 and Figure 5.20 show effect of particle shear stress term on turbulence intensity prediction. Again, significant improvement can be observed by comparing standard k-ε computed turbulence intensity in Figure 5.19 against Figure 5.13 and Figure 5.20 against Figure 5.14. Computed turbulence intensity in Figure 5.19 is lower than standard k-ε model computed data in Figure 5.13 for entire of pipe cross section and closer to experimental data. Computed turbulence intensities in Figure 5.20 are also lower than standard k-ε model computed turbulence intensities in Figure 5.14. Turbulence intensity computation of standard k-ε employed model excluding particle shear stress term which was previously found insensible to the presence of particles are now drastically improved. Turbulence intensity profiles computed by standard k-ε employed model itself cannot be sensible to the presence of particles but particle shear stress term affects to both gas and particle phase velocities, as a result, turbulence intensities are adjusted indirectly.

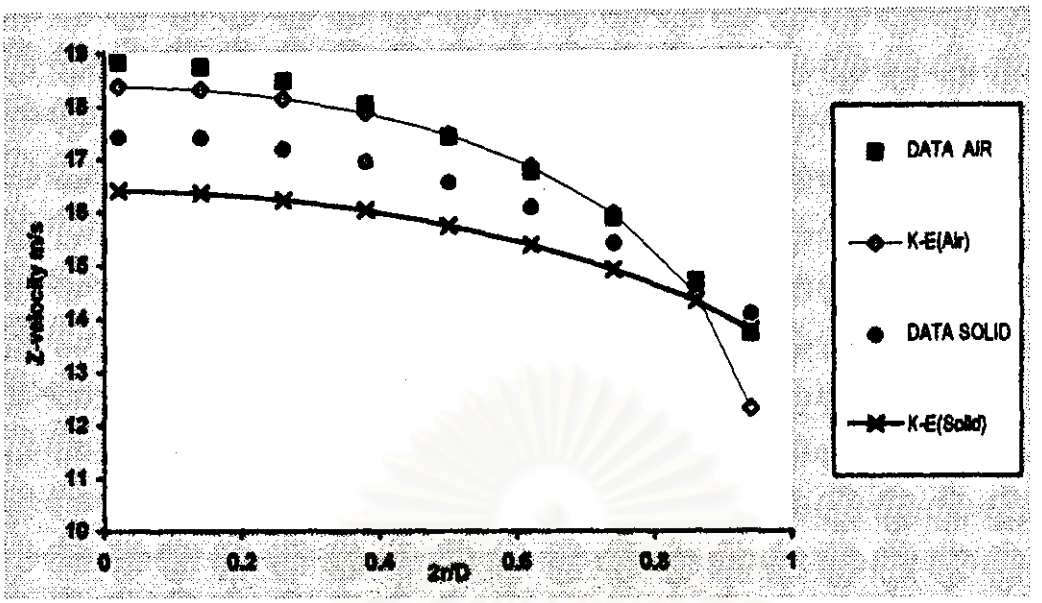

Figure 5.15
Axial velocity profile on radial variation of mean air velocity =15.6 m/s laden with 200μm. particles at solid loading ratio=1.0 , meaning of data legend: Data air and Data solid from Tsuji et.al [1984]'s experimental data, KE(Air) and KE(Solid) are computed value using standard k-ε model. Particle shear stress term is included in computation.

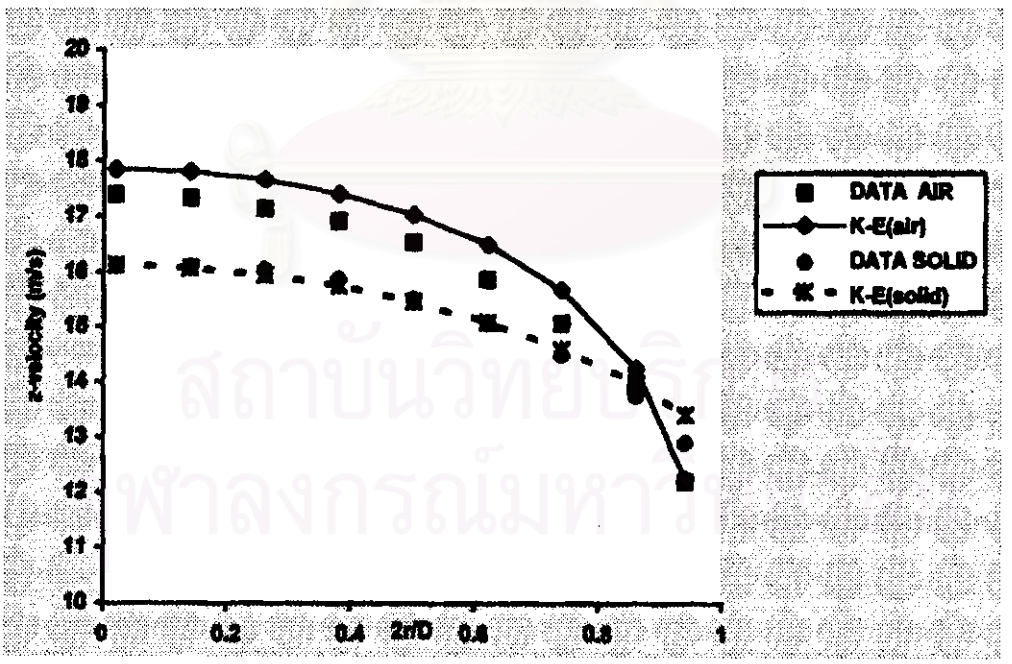

Figure 5.16
Axial velocity profile on radial variation of mean air velocity =15.3 m/s laden with 200μm. particle at solid loading ratio=2.1 , meaning of data legend: Data air and Data solid from Tsuji et.al [1984]'s experimental data, KE(Air) and KE(Solid) are computed value using standard k-ε model. Particle shear stress term is included in computation

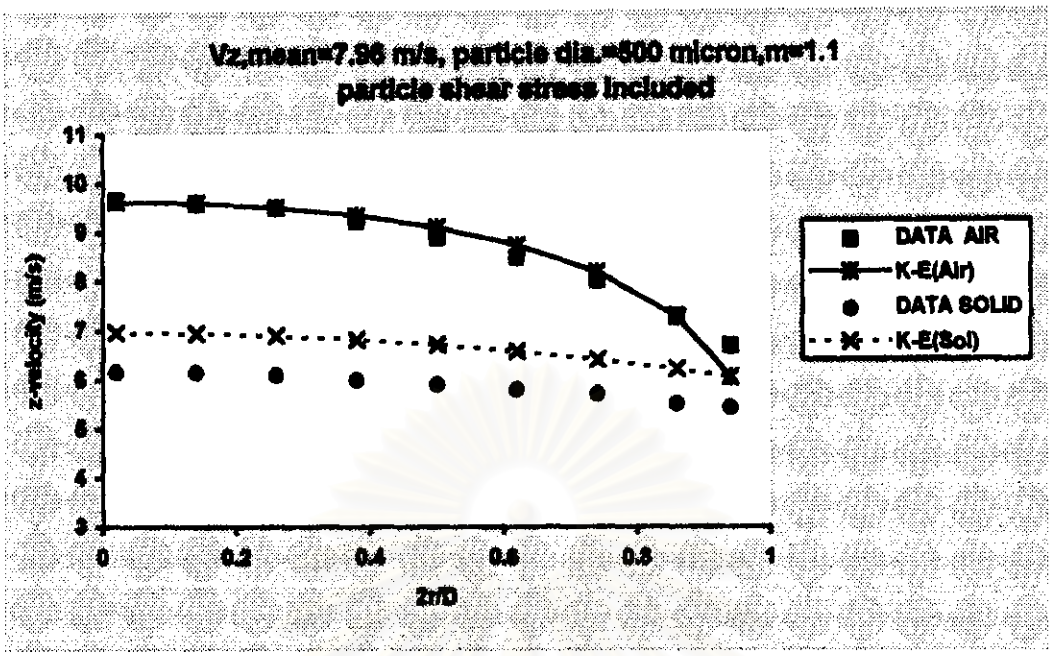

Figure 5.17

Axial velocity profile on radial variation of mean air velocity =7.96 m/s laden with 500μm. particle at solid loading ratio=1.1 , meaning of data legend: Data air and Data solid from Tsuji et.al [1984]'s experimental data, KE(Air) and KE(Solid) are computed value using standard k-ε model. Particle shear stress term is included in computation.

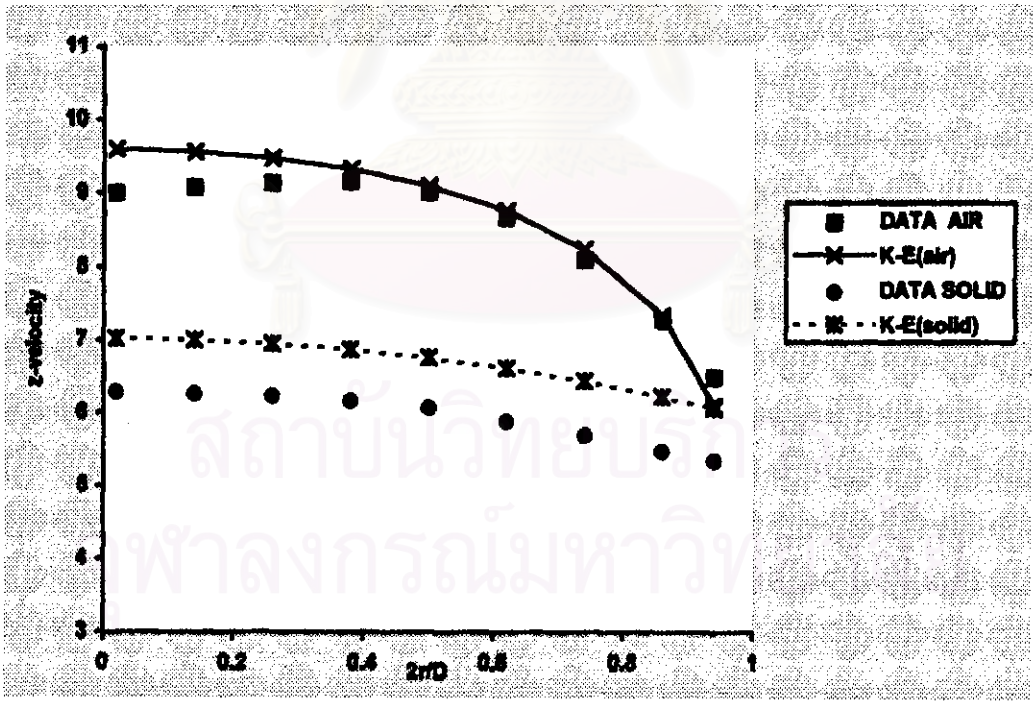

Figure 5.18

Axial velocity profile on radial variation of mean air velocity =8.00 m/s laden with 500μm. particle at solid loading ratio=2.0 , meaning of data legend: Data air and Data solid from Tsuji et.al [1984]'s experimental data, KE(Air) and KE(Solid) are computed value using standard k-ε model. Particle shear stress term is included in computation

In predicting axial pressure drop profile of experimental data shown in Figure 5.6, particle velocity at the test section inlet must be accurately specified. With the known slope of pressure drop curve at pipe inlet in Figure 5.6, the $\frac{dp(0)}{dz}$ in equation (3.46) can be assumed equal to such slope. Substitute equation (3.49) in to equation (3.46) together with $\frac{dp(0)}{dz}$, inlet particle velocity can then be solved.

Figure 5.21 and Figure 5.22 show the prediction of pressure drop profile. Computed particle inlet velocity are 6.55 m/s for $\bar{V}_t$=11.59 m/s and 9.31 m/s for $\bar{V}_t$=17.18 m/s . The standard k-ε employed flow model including particle shear stress term computation yield the computed pressure drop profiles plotted in Figure 5.21 and Figure 5.22. The computed profiles are in agreement with the experimental data. Validity of model in predicting pressure drop profile implies that mean volume fraction of both phases are accurately described since gas phase volume fraction gradient is proportionate to total pressure drop gradient as can be analysed by some manipulation of equation (3.1), (3.2) and (3.3).

5.2.5 Model validation : compare with other literature

Published data of Louge et al. [1991] are plotted against computed results of the model employed in Section 5.2.4 as shown in Figure 5.23, Figure 5.24 for velocity profile and Figure 5.25, Figure 5.26 for turbulence intensities. The objective is to investigate particle wall interaction effect which is investigated in Louge et al. [1991] but ignored in this study. Particle shear stress term is included in Louge et al. [1991] computation. Their mathematical model is based on kinetic theory of granular flow where additional granular temperature equation is introduced. In Figure 5.23, particle velocity profile of 200 μm computed by Louge et al. [1991] exhibit a straight line. The same trend can be investigated from Figure 5.24 for 500 μm particles. These evidence indicate the strength of particle shear stress term based on kinetic theory of granular flow which is proven successful in predicting wide range of gas-particle flow condition especially in rather dense flow which particle recirculation phenomena plays an important role. In this rather dilute flow,the validated model discussed in Section 5.2.4 appear to be advantage in predicting axial air and particle velocity profiles at least in the range studied.

Turbulence intensities computed by Louge et.al [1991] are plotted in Figure 5.25 and Figure 5.26 against computed results of the validated model discussed in Section 5.2.4. Both perform level, good prediction of turbulence intensity.

Adverse effect of ignoring particle wall interaction in computation could not be observed. Louge et al. [1991]'s model does not show superior performance in prediction of air, particle velocities and turbulence intensities in near-wall region over this validated model.

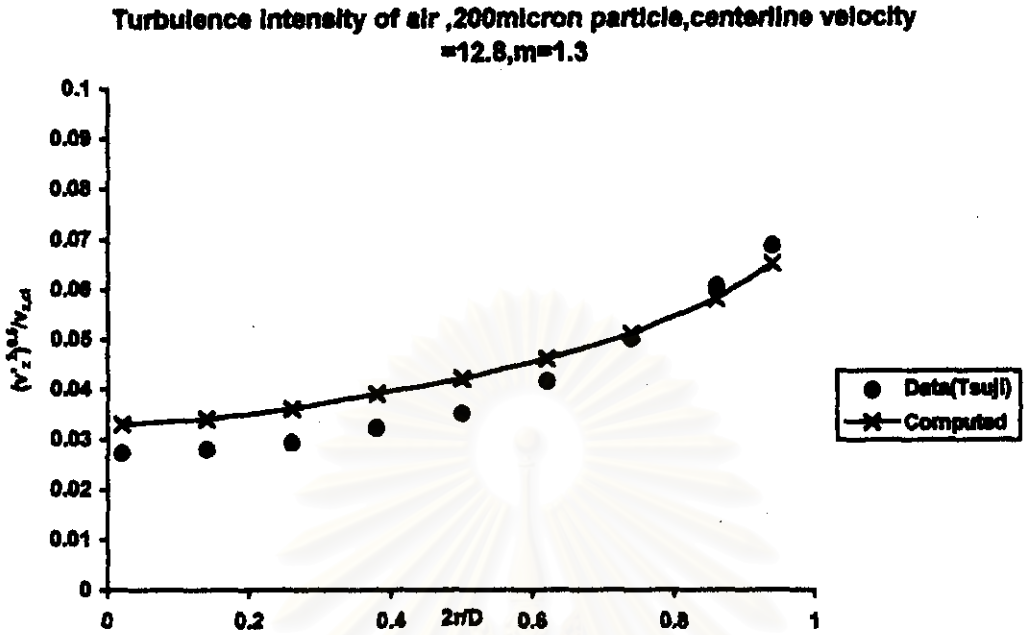

Figure 5.19

Turbulence intensity on radial variation of air in pipe flow laden with 200μm particles, centerline velocity=12.8 m/s, Data legend: **Tsuji's** is Tsuji et al. [1984]'s experimental data , **computed** is computed result using standard k-ε model and including particle shear stress term.

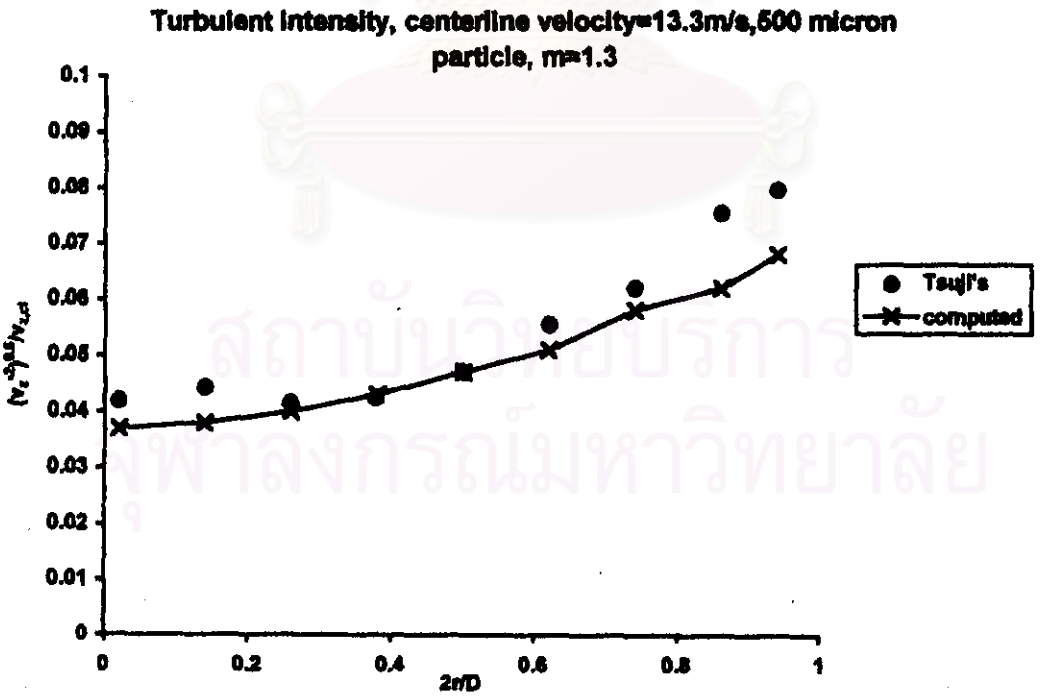

Figure 5.20

Turbulence intensity on radial variation of air in pipe flow laden with 500μm particles, centerline velocity=13.3 m/s, Data legend: **Tsuji's** is Tsuji et al. [1984]'s experimental data , **computed** is computed result using standard k-ε model and including particle shear stress term.

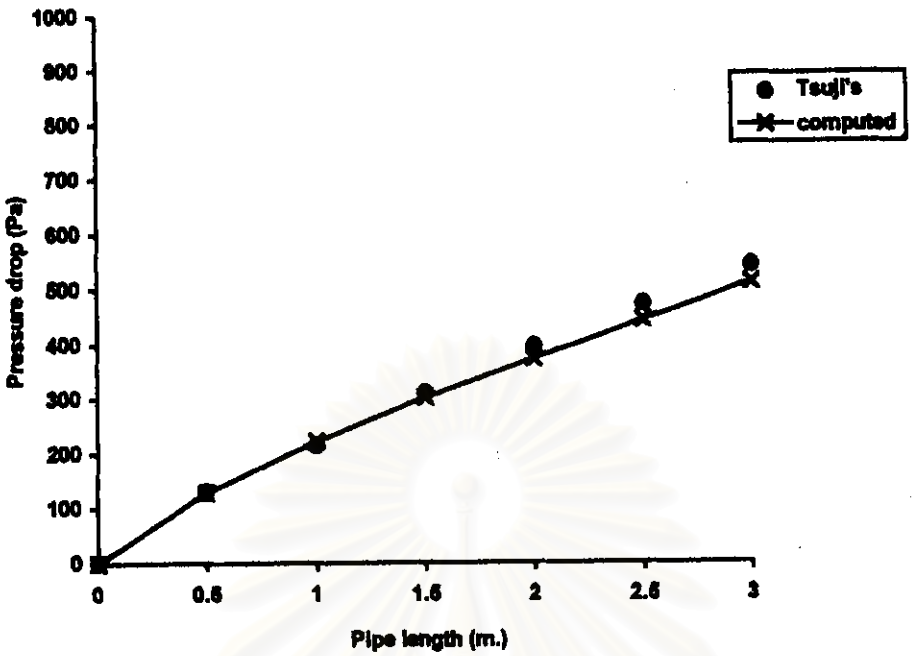

Figure 5.21

Pressure drop profile of air-solid mixture in pipe flow, mean air velocity=14.59 m/s, 500μm particles, mass flow rate =3×10^{-2}kg/s. Data legend: **Tsuji's** is Tsuji et al. [1984]'s experimental data, **computed** is the computed value using the standard k-ε model including particle shear stress term.

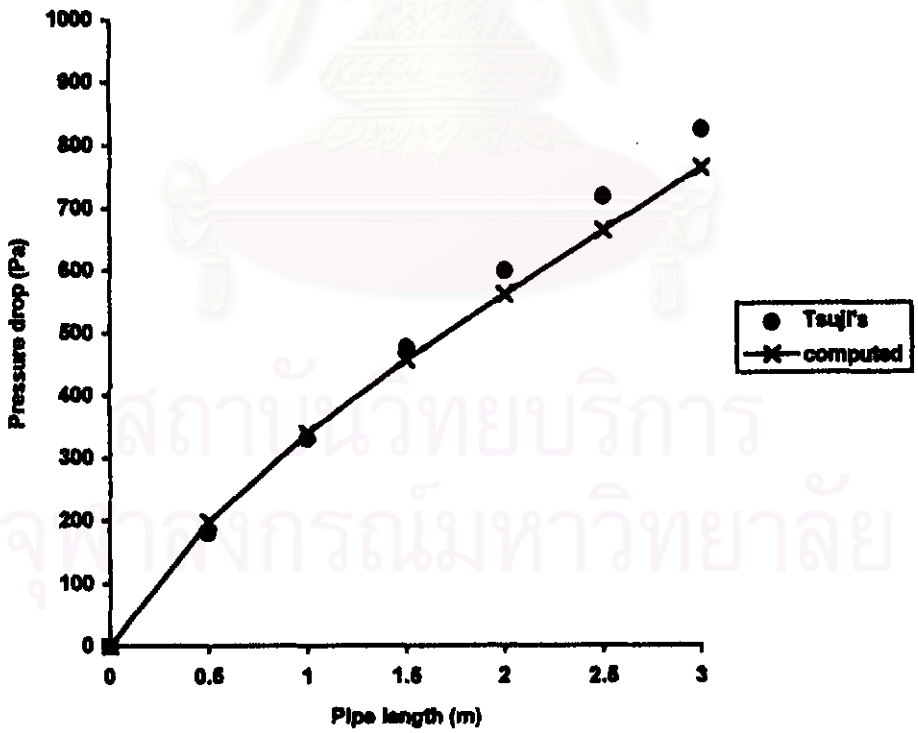

Figure 5.22

Pressure drop profile of air-solid mixture in pipe flow, mean air velocity=17.18 m/s, 500μm particles, mass flow rate =3×10^{-2}kg/s. Data legend: **Tsuji's** is Tsuji et al. [1984]'s experimental data, **computed** is the computed value using the standard k-ε model including particle shear stress term.

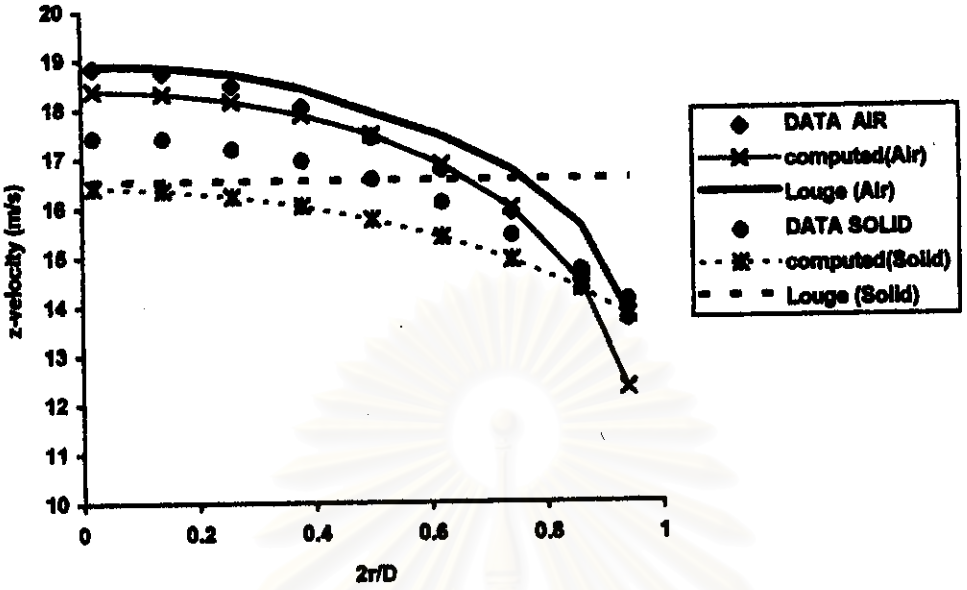

Figure 5.23

Axial velocity profile on radial variation of air velocity laden with 200μm particles at solid loading ratio =1.0, meaning of data legend: **DATA AIR** and **DATA SOLID** from Tsuji et al. [1984]'s experimental data: **KE(air)** and **KE (solid)** are the same as legend in figure 5.15. **Louge (air)** and **Louge (solid)** are the computed results of Louge et al.[1991].

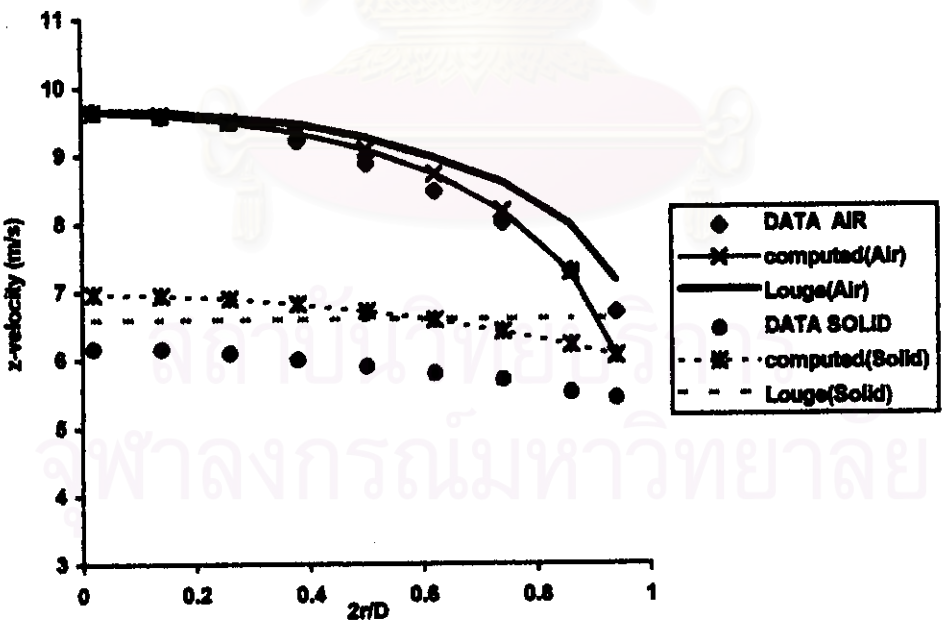

Figure 5.24

Axial velocity profile on radial variation of air velocity laden with 500μm particle at solid loading ratio =1.1, meaning of data legend: **DATA AIR** and **DATA SOLID** from Tsuji et al. [1984]'s experimental data: **KE(air)** and **KE (solid)** are the same as legend in figure 5.16. **Louge (air)** and **Louge (solid)** are the computed results of Louge et al.[1991].

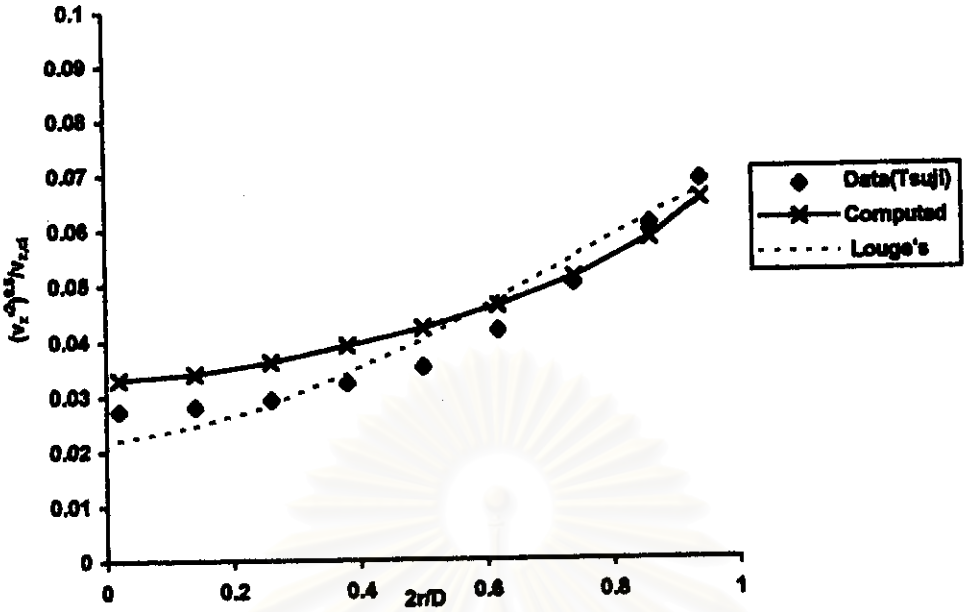

Figure 5.25

Turbulence intensity on radial variation of air in pipe flow laden with 200μm particles, centerline velocity=12.8,m=1.3 Data legend: **Tsuji's** is Tsuji et al. [1984]'s experimental data , **computed** is computed result using standard k-ε model and including particle shear stress term. **Louge's** is computed result of Louge et al. [1991].

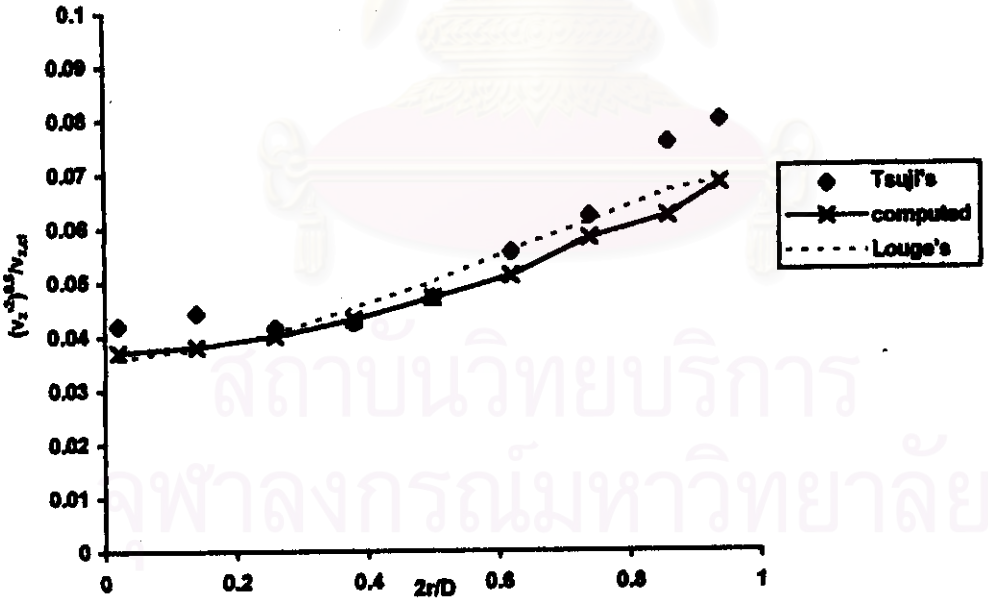

Figure 5.26

Turbulence intensity on radial variation of air in pipe flow laden with 500μm particles, centerline velocity=12.8, m=1.3, Data legend: **Tsuji's** is Tsuji et al. [1984]'s experimental data , **computed** is computed result using standard k-ε model and including particle shear stress term. **Louge's** is computed result of Louge et al. [1991].

5.2.6 The validated model

In conclusion, the validated model discussed in Section 4.2.4 will be employed to perform computation task in entire next chapter. However some aspect of the validated model need to be cautiously discussed here.

The validation of model is done base upon fully developed flow data. Gas phase turbulence viscosity and turbulence diffusivity of particulate phase are included in computation and its validity are proven. The remaining term which haven't been validated is turbulence phase mass diffusivity of particulate phase, D_t in equation (3.32) and (3.33) which is the same as present in Chen-Wood [1984]. Even though D_t expression has not been validated for 500μm particle, it has to be employed since little of such expression is available for this range of particle size.

Turbulence diffusivity property of particle in the range studied has been proven to be tightly dependent to turbulence kinetic energy and its dissipation rate of gas phase as seen in validated equation (3.32) and (3.33). The validity of model in predicting turbulence intensity profile of air indicate that the proposed turbulence phase mass diffusivity expression can be employed in simulation, at least in qualitative way.